Séminaire Poincaré 1 (2005) 95 – 113



# Decoherence of a Quantum Bit Circuit

G. Ithier, F. Nguyen, E. Collin, N. Boulant, P.J. Meeson, P. Joyez, D. Vion, and D. Esteve
Quantronics, SPEC, CEA-Saclay, F91191 Gif-sur-Yvette

## 1 Why solid state quantum bit circuits ?

These notes provide an introduction to the solid state quantum electrical circuits developed during recent years, following recent propositions for quantum machines. If no quantum-classical frontier indeed exists between the microscopic world and the macroscopic one, quantum machines could indeed take advantage of the richness of quantum physics for performing specific tasks more efficiently than classical ones. Although no quantum machine has been operated yet, probing quantum mechanics with collective variables involving a large number of underlying microscopic degrees of freedom is already an important goal. As expected, decoherence plays there an important role. We present here the systematic investigation carried out on the quantronium circuit developed by our team.

## 2 Towards quantum machines

Very interesting propositions for truly quantum machines, in which state variables are ruled by quantum mechanics, appeared in the domain of processors after Deutsch and Josza showed that the concept of algorithmic complexity is hardware dependent. It was shown that a simple set of unitary operations on an ensemble of coupled two level systems, called quantum bits (qubits), is sufficient to perform some specific computing tasks in a smaller number of algorithmic steps than with a classical processor [1]. Quantum algorithms furthermore solve some mathematical tasks presently considered as intractable, such as the factorisation of large numbers, exponentially faster than classical algorithms operated on sequential Von Neumann computers. Solid state quantum bit circuits are a new type of electronic circuits that aim at implementing quantum bits and quantum processors.

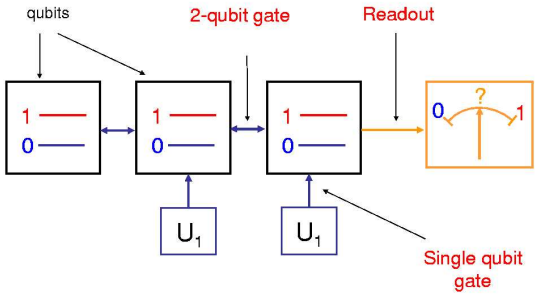


Figure 1: A quantum processor consists of an array of qubits. Logic operations are performed by controlling the single and two qubit Hamiltonians.

A sketch of a quantum processor is shown in Fig. 1. Each qubit is controlled independently, so that any unitary operation can be applied to it. Qubits are coupled in a controlled way so that all the two qubit gate operations required by algorithms can be performed. A two-qubit gate is universal when, combined with a subset of single qubit gates, it allows implemention of any unitary

evolution[1]. For instance, the control-not gate (C-NOT), which applies a not operation on qubit 2 when qubit 1 is in state 1, is universal.

### 2.1 Criteria required for qubits

Not all two level systems are suitable for implementing qubits. A series of points, summarised by DiVicenzo, need to be addressed (see chapter 7 in[1]):

1) The level spectrum should be sufficiently anharmonic to provide a good two level system.

2) An operation corresponding to a 'reset' is needed.

3) The quantum coherence time must be sufficient for the implementation of quantum error correction codes. This requirement is extremely demanding: less than one error in $10^4$ gate operations in the most optimistic case.

4) The qubits must be of a scalable design with a universal set of gates.

5) A high fidelity readout method is needed.

### 2.2 Qubit implementation: Atoms and ions versus electrical circuits

On the experimental side, implementing a quantum processor fullfilling these criteria is a formidable task [2]. The activity has been focused on the operation of simple systems, with at most a few qubits. Two main roads have been followed. Microscopic quantum systems like atoms[3] and ions[4] have been considered. Their main advantage is their excellent quantum coherence, but their scalability is questionable. The most advanced qubit implementation is based on ions in linear traps, coupled to their longitudinal motion [4] and addressed optically.

Solid state electrical circuits have attracted a large interest because they are considered as more versatile and more easily scalable, although reaching the quantum regime is extremely difficult. in this course, we provide a simple presentation of solid state qubits (see refs. [5, 6, 7, 8] for further reading on solid state qubit circuits).

### 2.3 Solid state electrical qubit circuits

Two main strategies based on quantum states of either single particles or of a whole circuit, have been followed for making solid-state electrical qubits.

In the first strategy, the quantum states are nuclear spin states, single electron spin states, or single electron orbital states. The advantage of using microscopic states is that their quantum behaviour has already been probed and can be excellent at low temperature. The main drawback is that qubit operations are difficult to perform since single particles are not easily controlled and read out.

The second strategy has been developed in superconducting circuits based on Josephson junctions, which form a kind of artificial atoms. Their Hamiltonian can be tailored almost at will, and a direct electrical readout can be incorporated in the circuit. On the other hand, these artificial atoms are less quantum than natural ones and spin degrees of freedom.

## 3 qubits based on semiconductor structures

Different types of quantum states suitable for making qubits can be found in semiconductor nanostructures, as described below. Two families can be distinguished: the first one being based on quantum states of nuclear spins, or of localised electrons, while the second one is based on propagating electronic states (flying qubits).

### 3.1 Kane's proposal: nuclear spins of P impurities in silicon

Kane's proposal, sketched in fig.2, is based on the S=1/2 nuclear spins of $P^{31}$ impurities in silicon [9]. The qubits are controlled through the hyperfine interaction between the nucleus of the $P^{31}$ impurity and the bound electron around it. The transition frequency of each qubit is determined by the magnetic field applied to it, and by its hyperfine coupling controlled by a gate

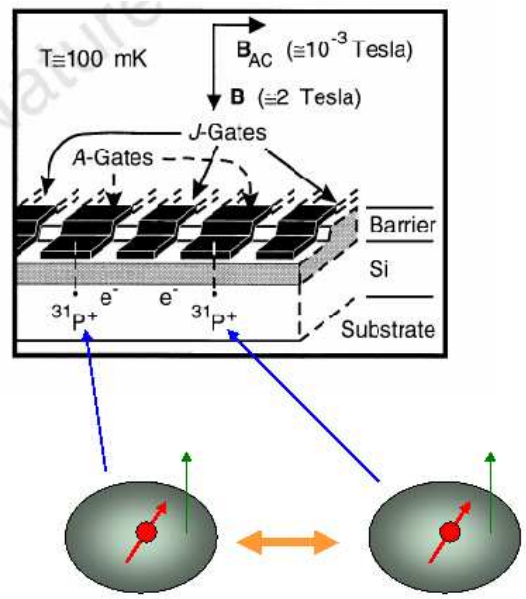


Figure 2: Kane's proposal: nuclear spins of phosphorus impurities form the qubits. The control is provided by the hyperfine interaction with a bound electron around each impurity. Each qubit is controlled by applying a voltage to an A gate electrode that displaces slightly the wavefunction of the bound electron, and thus modifies the hyperfine interaction. The two qubit operations are performed using the J gates, which control the exchange interaction between neighboring bound electrons, and thus the interaction between the qubits. *(picture taken from[9].)*

voltage (A gates). The exchange interaction between the electrons mediates an effective interactions between the qubits, which can be also controlled by a gate voltage (J gate). Single qubit gates would be performed by using resonant pulses, like in NMR, while two qubit gates would be performed using the J gates. The readout would be performed by transfering the information on the qubit state to the charge of a quantum dot, which would then be read using an electrometer. The feasibility of this seducing proposal still has to be demonstrated.

### 3.2 Charge states in quantum dots

Although the occupation of a quantum dot by a single electron is not expected to provide an excellent qubit because the electron strongly interacts with electric fields, coherent oscillations in a semiconductor qubit circuit[10] were observed by measuring the transport current in a double dot, as shown in Fig. 3. Recently, a coherence time of the order of 200 ns was achieved in a similar double dot structure, using a single electron transistor (SET) for the qubit readout. [11].

### 3.3 Electron spins in quantum dots

Using electron spins for the qubits is attractive because the spin is weakly coupled to the other degrees of freedom of the circuit, and because the spin state can be transferred to a charge state for the purpose of readout (see [12] and refs. therein). The device shown in Fig. 4 is a double dot in which the exchange interaction between the single electrons in the dots is controlled by the central gate voltage. The readout is performed by monitoring the charge of the dot with a quantum point contact transistor close to it: first, the dot gate voltage is changed so that an up spin electron stays in the dot, while a down spin electron leaves it. In that case, another up spin electron from the reservoir can enter the dot. The detection of changes in the dot charge then provides a single shot efficient measurement of the qubit state [12].

Another setup based on a similar double-dot structure, was recently proposed [13]. In this

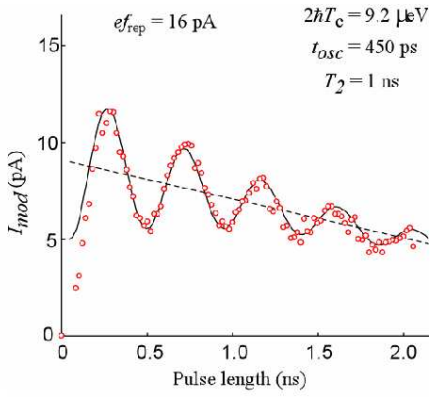


Figure 3: oherent oscillations of a single electron inside a double dot structure, as a function of the duration of a dc pulse applied to the transport voltage. These oscillations are revealed by the average current when the pulse is repeated at a large rate *(picture taken from Hayashi et al.[10] )*

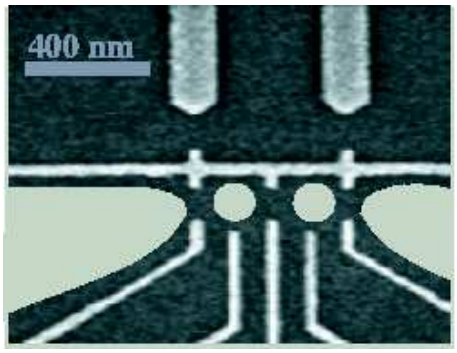


Figure 4: Scanning Electron Micrograph of a double dot implementing two qubits . The qubits are based on the spin of a single electron in the ground state of each dot (disks). *(Courtesy of Lieven Vandersypen, T.U. Delft).*

new scheme, the qubit is encoded in the spin of two electron states with one electron charge in each dot. These spin states are the singlet $S$ state and the triplet $T$ state $m = 0$. Coherent qubit manipulation was achieved by controlling the exchange interaction between the two dots. Although the coherence time was limited at about 10 ns due to the magnetic field produced by the nuclei in the substrate, coherent signals were recovered at times 1 $\mu$s using echo methods, like in NMR.

### 3.4 Flying qubits

Propagating electron states have also been proposed for implementing qubits. Propagating states in wires with a small number of conduction channels have been considered, but edge states in Quantum hall Effect structures seem to offer a better solution [5] because of their long phase coherence time at low temperature. Qubit states could then be encoded using electrons propagating in opposite directions, along the opposite sides of the wires.

## 4 Superconducting qubit circuits

The interest of using the quantum states of a whole circuit for implementing qubits is to benefit from the wide range of Hamiltonians that can be obtained when inductors and capacitors are combined with Josephson junctions, which provide the anharmonicity required for making two level systems. Josephson qubit circuits can be considered as artificial macroscopic atoms, whose

properties can be tailored. Their Hamiltonian can be controlled by applying electric or magnetic fields, and bias currents.

### 4.1 Hamiltonian of Josephson circuits

When branch variables are chosen, the contribution to the Hamiltonian of a Josephson element in a given branch is:

$$h(\theta) = -E_J \cos(\theta),$$

where $\theta$ is the superconducting phase difference across the junction, $E_J = I_0\varphi_0$ the Josephson energy, with $I_0$ the critical current of the junction, and $\varphi_0 = \hbar/2e$. The phase $\theta$ is the conjugate of the number $N$ of Cooper pairs passed across the junction. The full Hamiltonian is then obtained by adding the electromagnetic terms to the Josephson terms [14, 15]. Any junction in a circuit is characterised by the fluctuations of $\theta$ and of $N$. Often, the circuit junctions are either in the phase or number regimes, characterised by small and large fluctuations of the phase, respectively. Qubit circuits can be classified according to the regime to which they belong. The main types of superconducting qubit circuits can be classified along a phase to charge axis, as shown in Fig. 5.

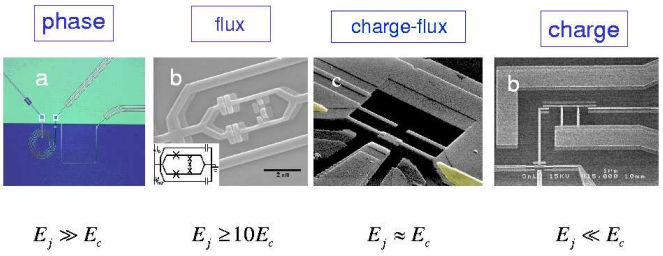


Figure 5: Left: A Cooper-pair box consists of a small superconducting island connected by a Josephson junction to a superconducting reservoir, and charge biased by a gate capacitance connected to a voltage source. Right: schematic circuit. The Josephson coupling allows the exchange of Cooper pairs. The phase of the superconducting island and the number of extra Cooper pairs inside are conjugated variables.

The phase qubit[16] developed at NIST (Boulder) consists of a Josephson junction in a flux biased loop, and the Josephson potential has two wells. The qubit states are two quantized levels in the first potential well, and the readout is performed by resonantly inducing the transfer to the second well, using a monitoring SQUID to detect it.

The flux qubit[17, 18] developed at T.U. Delft consists of three junctions in a loop, placed in the phase regime. Its Hamiltonian is controlled by the flux threading the loop. The flux qubit can be coupled in different ways to a readout SQUID. This circuit is in the phase regime.

The quantronium circuit[19, 20, 8, 21], developed at CEA-Saclay is operated in the intermediate charge-phase regime. The Cooper pair box[23], operated in the charge regime at NEC, is the first qubit circuit for which coherent control of the quantum state was achieved [22]. A detailed description of all Josephson qubits, with extensive references to other works, is given in [6, 7, 8].

### 4.2 The Cooper pair box

The single Cooper pair box[8] consists of a single junction connected to a voltage source across a small gate capacitor, as shown in Fig. 6. Its Hamiltonian writes:

$$\widehat{H}(N_g) = E_C(\widehat{N} - N_g)^2 - E_J \cos\widehat{\theta} \quad (1)$$

where $E_C = (2e)^2/2C_\Sigma$ is the charging energy of a cooper pair in the island, and $N_g = C_g V_g/(2e)$ the reduced gate charge with $V_g$ the gate voltage. The operators $\widehat{N}$ and $\widehat{\theta}$ obey the commutation

relation $\left[\widehat{\theta}, \widehat{N}\right] = i$. The energy spectrum can be analytically determined, and is $2e$ periodic with the gate charge. When $E_J \ll E_C$, and at $N_g \equiv 1/2 mod[1]$, the qubit states are simply symmetric and antisymmetric combinations of successive $|N\rangle$ states.

The most direct way to probe the Cooper pair box is to measure the island charge. After the measurement of the island charge in the ground state [23] with an electrometer based on a Single Electron Transistor (SET) [24], the first Josephson qubit experiment was performed by monitoring the current through an extra junction connected on one side to the box island and on the other side to a voltage source [22]. A charge readout of a Cooper pair box [25] using a rf-SET [26], and a single-shot high fidelity sample and hold readout [27] were later obtained. Finally, a Cooper pair box embedded in a resonant microwave cavity, similar to an atom in a cavity [3], was recently operated [28].

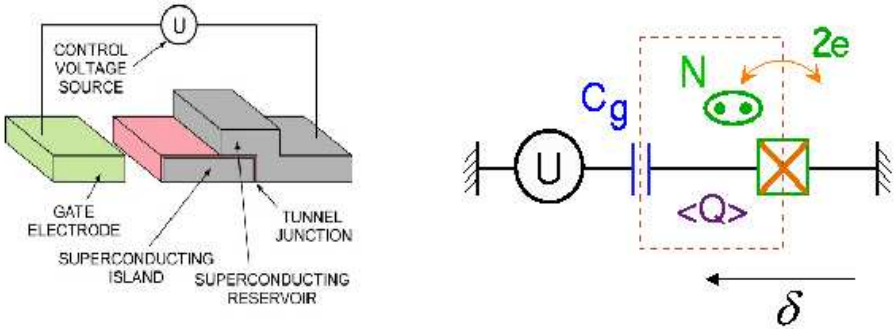


Figure 6: The Cooper pair box consists of a small superconducting island connected to a superconducting reservoir, by a Josephson junction (crossed square in the electrical scheme), and biased by a gate capacitor. The Josephson coupling allows the exchange of Cooper pairs between the island and the reservoir. The island phase and the extra number of Cooper pairs in the island are conjugated variables.

### 4.3 How to maintain quantum coherence?

When the readout circuit measures the qubit, its backaction results in full qubit decoherence during the time needed to get the outcome, and even faster if the readout efficiency is below the quantum limit. In order to reduce decoherence, the readout circuit should thus be switched off when the qubit is operated, and switched on just at readout time. Before explaining a possible strategy to circumvent this problem, we expose the basic concepts underlying decoherence in qubit circuits.

The interaction between a qubit and the degrees of freedom of its environment entangles both parties. This entanglement takes a simple form in the weak coupling regime, which is usually the case in qubit circuits[29]. The control parameters of the qubit Hamiltonian ( such as $N_g$ for the Cooper pair box), are in fact dynamical variables of the qubit environment, which can fluctuate.

### 4.4 Qubit-environment coupling Hamiltonian

We call $\lambda$ the set of control variables entering the Hamiltonian of a qubit. At a given working point $\lambda_0$, the qubit space is analogous to a fictitious spin 1/2 with $\sigma_z$ eigenstates $|0\rangle$ and $|1\rangle$. Using the Pauli matrix representation of spin operators, the expansion of the Hamiltonian around $\lambda_0$ yields the coupling Hamiltonian:

$$\widehat{H}_X = -1/2 \left(\overrightarrow{D}_\lambda \cdot \overrightarrow{\sigma}\right) \left(\widehat{\lambda} - \lambda_0\right) \tag{2}$$

where $\overrightarrow{D}_\lambda \cdot \overrightarrow{\sigma}$ is the restriction of $-2\widehat{\partial H/\partial \lambda}$ to the $\{|0\rangle, |1\rangle\}$ space. This coupling Hamiltonian determines the qubit evolution when a control parameter is varied,and thus the coupling to decoherence noise sources.

In the weak coupling regime, the fluctuations of the qubit environment are characterised by the spectral density:

$$S_{\lambda_0}(\omega) = \frac{1}{2\pi}\int_{-\infty}^{+\infty} d\tau \left\langle \left(\widehat{\lambda}(t) - \lambda_0\right)\left(\widehat{\lambda}(t+\tau) - \lambda_0\right)\right\rangle \exp(-\mathbf{i}\omega\tau) \tag{3}$$

This spectral density is defined for positive and negative $\omega'$s, proportional to the number of environmental modes that can absorb and emit a quantum $\hbar\omega$, respectively. In the case of the Cooper pair box, the fluctuations of the gate charge $N_g$ arise from the impedance of the biasing circuitry and from microscopic charge fluctuators in the vicinity of the box island[8, 21].

### 4.5 Relaxation

The decay of the diagonal part of the density matrix in the eigenstate basis $\{|0\rangle, |1\rangle\}$ involves $|1\rangle \rightarrow |0\rangle$ qubit transitions, with the energy transferred to the environment. Such an event resets the qubit in its ground state. The decay is exponential, with a rate:

$$\Gamma_1 = \frac{\pi}{2}\left(\frac{D_{\lambda,\perp}}{\hbar}\right)^2 S_{\lambda_0}(\omega_{01}) \ . \tag{4}$$

The symbol $\perp$ indicates that only transverse fluctuations at positive frequency $\omega_{01}$ induce downward transitions. Upward transitions, which involve $S_{\lambda_0}(-\omega_{01})$, occur at a negligible rate for experiments performed at temperatures $k_B T \ll \hbar\omega_{01}$, provided the environment is at thermal equilibrium. The relaxation time is thus $T_1 = 1/\Gamma_1$.

### 4.6 Decoherence= relaxation + dephasing

When a coherent superposition $a|0\rangle + b|1\rangle$ is prepared, the amplitudes $a$ and $b$ evolve in time, and the non diagonal part of the density matrix oscillates at the qubit frequency $\omega_{01}$. The precise definition of decoherence is the decay of this part of the density matrix. There are two distinct contributions to this decay. Relaxation contributes to decoherence by an exponential damping factor with a rate $\Gamma_1/2$, but another process, called dephasing, often dominates. When the qubit frequency $\Omega_{01}$ fluctuates, an extra phase factor $\exp[i\Delta\varphi(t)]$ with $\Delta\varphi(t) = \frac{D_{\lambda,z}}{\hbar}\int_0^t \left(\widehat{\lambda}(t') - \lambda_0\right) dt'$ builds up between both amplitudes, the coupling coefficient $D_{\lambda,z}$ being:

$$D_{\lambda,z} = \langle 0|\,\widehat{\partial H/\partial\lambda}\,|0\rangle - \langle 1|\,\widehat{\partial H/\partial\lambda}\,|1\rangle = \hbar\partial\omega_{01}/\partial\lambda \ .$$

Dephasing thus involves longitudinal fluctuations, and contributes to decoherence by the factor:

$$f_X(t) = \langle \exp[i\Delta\varphi(t)]\rangle \ . \tag{5}$$

This dephasing factor $f_X(t)$ is not necessarily exponential. When $D_{\lambda,z} \neq 0$ , and assuming a gaussian process for $\left(\widehat{\lambda}(t') - \lambda_0\right)$, one finds using a semi-classical approach:

$$f_X(t) = \exp\left[-\frac{t^2}{2}\left(\frac{D_{\lambda,z}}{\hbar}\right)^2 \int_{-\infty}^{+\infty} d\omega \ S_{\lambda_0}(\omega)\mathrm{sinc}^2(\frac{\omega t}{2})\right] \ , \tag{6}$$

which is justified by a full quantum treatment of the coupling to a bath of harmonic oscillators justifies using the quantum spectral density in the above expression [21, 29].

### 4.7 The optimal working point strategy

The above considerations on decoherence yield the following requirements for the working point of a qubit:

-In order to minimize the relaxation, the coefficients $D_{\lambda,\perp}$ should be small, and ideally $D_{\lambda,\perp} = 0$.

-In order to minimize dephasing, the coefficients $D_{\lambda,z} \propto \partial\Omega_{01}/\partial\lambda$ should be small. The optimal case is when the transition frequency is stationary with respect to all control parameters: $D_{\lambda,z} = 0$. At such optimal points, the qubit is decoupled to first order from its environment and from the readout circuitry. This means that the two qubit states cannot be discriminated at an optimal point. One must therefore depart in some way from the optimal point in order to perform the readout.

## 5 The quantronium circuit

The optimal working point strategy was first applied to the Cooper pair box, with the quantronium circuit [19, 20, 8].

The quantronium circuit, shown in fig. 7, is derived from the Cooper pair box. The box Josephson junction is split into two junctions with respective Josephson energies $E_J(1 \pm d)/2$, with $d \in [0, 1]$ a small asymmetry coefficient. The reason for splitting the junction into two halves is to form a loop that can be biased by a magnetic flux $\Phi$. A third junction is inserted in the loop for the purpose of performing the readout of the qubit. A split box has two degrees of freedom, which can be chosen as the island phase $\widehat{\theta}$ and the phase difference $\widehat{\delta}$ across the two box junctions.

The phase difference $\widehat{\delta}$ in the split-box Hamiltonian is related to the phase difference across the readout junction by the relation $\widehat{\delta} = \widehat{\gamma} + \Phi/\phi_0$, where the phase $\widehat{\gamma}$ is the phase of the readout junction. Except at readout time, when the qubit gets entangled with the readout junction, $\widehat{\delta}$ can be considered as an almost classical parameter. The Hamiltonian of the split box alone, which depends on the two control parameters $N_g$ and $\delta$, writes:

$$\widehat{H} = E_C(\widehat{\mathbf{N}} - N_g)^2 - E_J \cos(\frac{\widehat{\delta}}{2}) \cos(\widehat{\theta}) + dE_J \sin(\frac{\widehat{\delta}}{2}) \sin(\widehat{\theta}) \ . \tag{7}$$

The corresponding energy levels can be calculated as a function of the control parameters[21]. The variations of the qubit transition frequency with the control parameters are shown in Fig.7. Different optimal points where all derivatives $\partial\Omega_{01}/\partial\lambda_i$ vanish are present.

The loop current operator provides a new variable to probe the qubit:

$$\widehat{I}(N_g, \delta) = (-2e) \left( -\frac{1}{\hbar} \frac{\partial \widehat{H}}{\partial \delta} \right) \ .$$

The average loop current $\langle i_k \rangle$ in state $|k\rangle$ obeys a generalized Josephson relation: $\langle i_k(N_g, \delta) \rangle = \left\langle k \left| \widehat{I} \right| k \right\rangle = \frac{1}{\varphi_0} \partial E_k(N_g, \delta)/\partial\delta$ . The difference between the loop currents of the two qubit states is $\Delta i_{10} = \langle i_1 \rangle - \langle i_0 \rangle = 2e\partial\omega_{10}/\partial\delta$. As expected, the difference $\Delta i_{10}$ vanishes at an optimal point.

### 5.1 Relaxation and dephasing in the quantronium

The split box is coupled to noise sources that affect the gate charge $N_g$ and the phase $\delta$ [8, 21]. The coupling to these noise sources $D_{\lambda,\perp}$ and $D_{\lambda,z}$ for relaxation and dephasing are obtained from the definition 2.

The coupling vector $D_{\lambda,\perp}$ for relaxation is:

$D_{\lambda,\perp} = \left\{ 4E_C \left| \left\langle 0 \left| \widehat{N} \right| 1 \right\rangle \right|, 2\varphi_0 \left| \left\langle 0 \left| \widehat{I} \right| 1 \right\rangle \right| \right\}$.

Relaxation can thus proceed through the charge and phase ports, but the phase port does not contribute to relaxation at $N_g = 1/2$ when the asymmetry factor $d$ vanishes. Precise balancing of the box junctions is thus important in the quantronium.

The coupling vector for dephasing is directly related to the derivatives of the transition frequency:

$D_{\lambda,z} = \hbar \ (\partial\omega_{01}/\partial N_g, \ \partial\omega_{01}/\partial\delta)$.

The charge noise arises from the noise in the gate bias circuit and from the background charge noise due to microscopic fluctuators in the vicinity of the box tunnel junctions. These noises have a $1/f$ spectral density at low frequency.

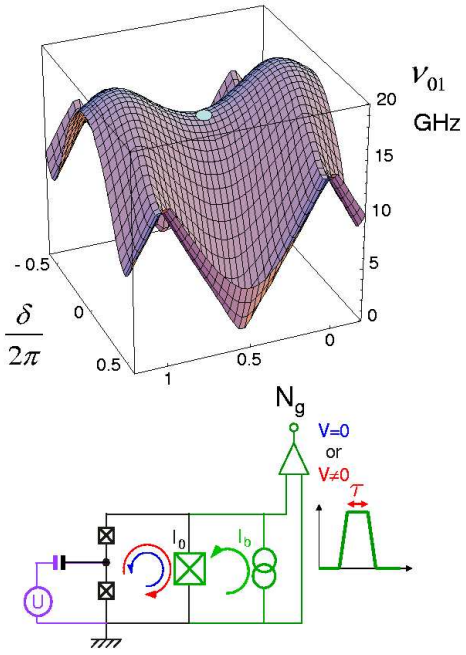


Figure 7: bottom: Schematic circuit of the quantronium qubit circuit. The quantronium consists of a readout junction inserted in the loop of a split-junction Cooper pair box. When a trapezoidal current pulse is applied, the readout junction switches to the voltage state with a larger probability for state $|1\rangle$ than for state $|0\rangle$. Top: Calculated transition frequency as a function of the control parameters $N_g$ and $\delta$ for the parameters $E_J = 0.86\ k_BK$, $E_C = 0.68\ k_BK$. The optimal point used in the experiments is the saddle point $(N_g = 1/2, \delta = 0)$

## 5.2 Readout of the quantronium

The readout junction can be used in different ways in order to discriminate the qubit states.

### 5.2.1 Switching readout

The simplest method consists in using the readout junction to perform a measurement of the loop current after adiabatically moving away from the optimal point. For this purpose, a trapezoidal readout pulse with a peak value slightly below the readout junction critical current is applied to the circuit(see fig. 7). Since this bias current adds to the loop current in the readout junction, the switching of the readout junction to a finite voltage state can be induced with a large probability for state $|1\rangle$ and with a small probability for state $|0\rangle$. This switching method is in principle a single shot readout. It has been applied to the quantronium[20] and to the flux qubit[18], with a switching probability difference up to 40% and 70%, respectively. The lack of fidelity is attributed to spurious relaxation during the readout bias current pulse. This switching method does not allow for a subsequent readout and is thus not quantum non demolition (QND).

### 5.2.2 AC methods for QND readout

Recently, microwave methods measuring the phase of a microwave signal reflected or transmitted by the circuit have been proposed for different superconducting qubits in order to attempt a non destructive QND readout. In general, with these rf methods, the working point stays, on average, at the optimal point, and undergoes small amplitude oscillations at a frequency different from

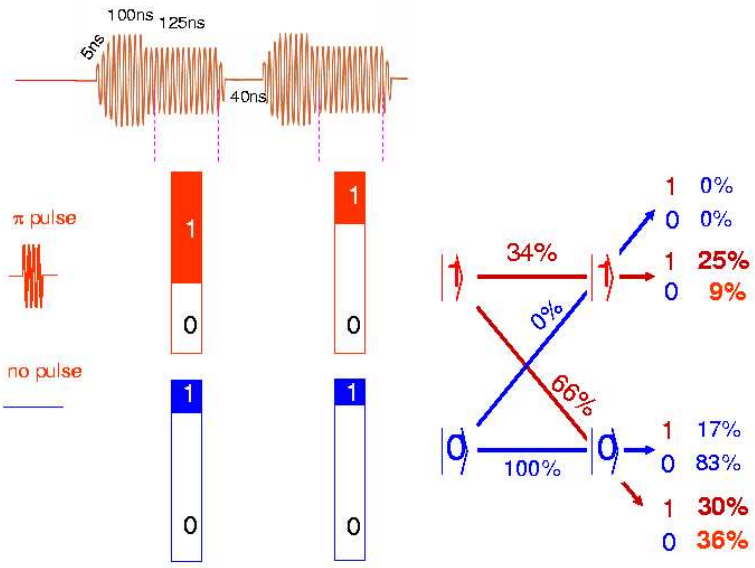


Figure 8: The statistics of successive readout outcomes, performed in the ground state and in the excited state of the qubit, give access to the QND fraction of the ac readout method developed for the quantronium. In this experiment, the readout fidelity and the QND fraction are rather low in the excited state of the qubit.

the qubit frequency. Avoiding relaxation when moving far away from the optimal point might furthermore improve the readout fidelity. Such methods have been proposed for the flux qubit[30], the quantronium[31, 32], and the Cooper pair box[28, 33]. In the quantronium, The qubit slightly modifies the inductance of the whole circuit[32], with opposite changes for the two qubit states. This change is inferred from the phase of the reflected signal,taking benefit of the non-linear resonance of the readout junction [31]. We have probed the QND character of this Josephson Bifurcation Amplifier (JBA) readout [32, 34] by comparing the outcomes of two successive readouts, as shown in Fig. 8. We found that the readout is only partly QND, and induces relaxation. Like in the case of the switching readout, spurious relaxation limits readout performances.

## 6 Coherent control of the qubit

Coherent control of a qubit is performed by driving the control parameters of the Hamiltonian. Although an adiabatic evolution is possible, most of experiments have been performed with hard pulses.

In the dc-pulse method[22], a sudden change of the Hamiltonian is performed. The qubit state does not in principle evolve during the change, but evolves afterwards with the new Hamiltonian during the pulse duration. This simple method requires extremely short pulse rise-times.

In the resonant pulse method, a control parameter is varied sinusoidally at the qubit frequency. When the gate voltage of a Cooper pair box is modulated by a resonant microwave pulse with amplitude $\delta N_G$, the Hamiltonian 2 contains a term $h(t) = -2E_C \left\langle 0 \left| \widehat{N} \right| 1 \right\rangle \sigma_X$, which induces Rabi precession at frequency:

$\omega_R = 4E_C \ \delta N_G \ /\hbar \left| \left\langle 0 \left| \widehat{N} \right| 1 \right\rangle \right|$.

As described in Fig. 9, the fictitious spin representing the qubit rotates around an axis located in the equatorial plane of the Bloch sphere, at an angle given by the phase of the microwave pulse. A single resonant pulse with duration $\tau$ induces a rotation by an angle $\omega_R \tau$, which manifests itself by oscillations of the switching probability, as shown in Fig. 9. When the pulse is not resonant, the detuning adds a $z$ component to the rotation vector.

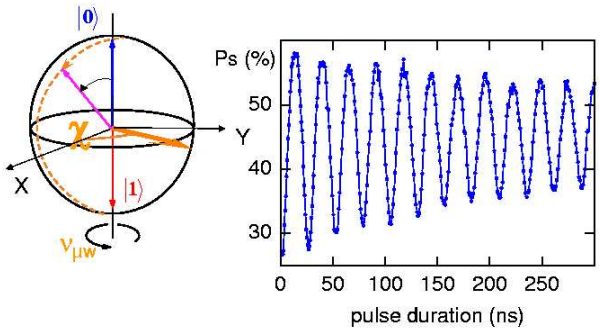


Figure 9: Left: Rabi precession of the qubit state represented on the Bloch sphere in the rotating frame during a resonant microwave pulse; right: Rabi oscillations of the switching probability with the pulse duration.

### 6.1 NMR-like control of a qubit

More complex manipulations inspired from NMR[35, 36, 37] have been performed in order to implement single qubit gates, and to probe decoherence processes[38, 39].

Three sequential rotations around two orthogonal axes, for instance the $x$ and $y$ axes on the Bloch sphere, allow to perform any unitary operation on a qubit. It is thus important to test whether or not two subsequent rotations combine as predicted, which is shown in Fig. 10. The

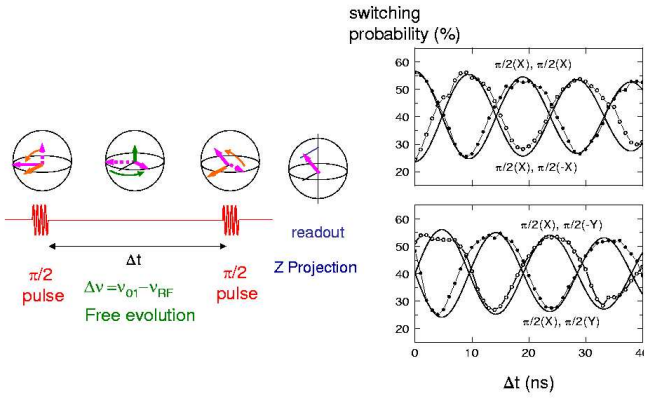


Figure 10: Switching probability after two $\pi/2$ pulses around two orthogonal axes, as a function of the delay between the pulses. The phase of the oscillating signal at the detuning frequency 50 MHz varies as predicted for the different combinations of rotation axes. The solid lines are theoretical fits *(taken from [39])*.

issue of gate robustness is also extremely important because the needs of quantum computing are extremely demanding. In NMR, composite pulse methods have been developed in order to make transformations less sensitive to pulse imperfections[36, 37, 40]. In these methods, a single pulse is replaced by a series of pulses that yield the same target operation, but with a decreased sensitivity to pulse imperfections. In the case of frequency detuning, a particular sequence named CORPSE (Compensation for Off-Resonance with a Pulse Sequence) has proved to be extremely efficient[40]. This sequence was probed in the quantronium for a $\pi$ rotation around the $X$ axis [39].

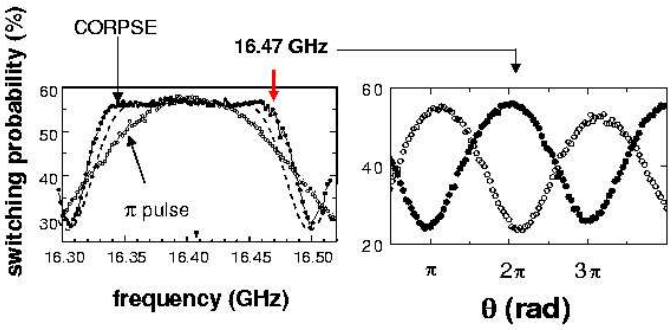


Figure 11: Left: switching probability after a single $\pi$ pulse (open symbols) and after a Corpse pulse corresponding to the same rotation (full symbols), as a function of frequency. The broad maximum for the CORPSE pulse proves the robustness respectively to frequency variations. Right: switching probability after a rotation by an angle theta around the $-X$ axis (open symbols), and after a subsequent CORPSE pulse (full symbols). The phase opposition between the two patterns indicates that the Corpse pulse works for any initial state;

## 7 Probing qubit coherence

We discuss now decoherence during the free evolution of the qubit, and during its driven evolution. Decoherence induces the decay of the qubit density matrix elements, both in the lab and rotating frames. As explained in section 4.6, decoherence is characterised by relaxation, affecting the diagonal and off diagonal parts of the density matrix, and by dephasing, which affects only its off diagonal part. Detailed explanations can be found in [41].

### 7.1 Relaxation

Relaxation is readily obtained from the decay of the signal after a $\pi$ pulse. The relaxation time in the quantronium ranges from a few hundreds of nanoseconds up to a few microseconds. These relaxation times are shorter than those calculated from the coupling to the external circuit using an estimated value for the asymmetry factor $d$. Excessive relaxation is found in all Josephson qubits, and could be attributed to the coupling with spurious microscopic two level systems, as suggested in [42].

### 7.2 Decoherence during free evolution

The most direct way to probe decoherence is to perform a Ramsey fringe experiment, as shown in Fig. 12, using two $\pi/2$ pulses slightly out of resonance. The first pulse creates a superposition of states, with an off diagonal density matrix. After a period of free evolution, during which decoherence takes place, a second pulse transforms part of the off-diagonal terms of the density matrix into a longitudinal term, which is measured by the subsequent readout pulse. The decay of the obtained oscillations at the detuning frequency characterize decoherence. This experiment was first performed in atomic physics, and it corresponds to the free induction decay (FID) in NMR. When the decay is not exponential, we define the coherence time as the time corresponding to a decay factor $\exp(-1)$. Other more sophisticated pulse methods have been developed to probe coherence. When the operating point is moved away from the optimal point at which decoherence is weak during a fraction of the delay between the two pulses of a Ramsey sequence, the signal gives access to decoherence at this new working point.

In order to better characterize decoherence, a series of experiments has been performed on the same sample whose decay of Ramsey interferences is shown in Fig. 13. This decay is not exponential, as expected from the so-called 'static' model[41] which assumes that frequency fluctuations responsable for dephasing are almost static on the time scale of each Ramsey pulse sequence. Other

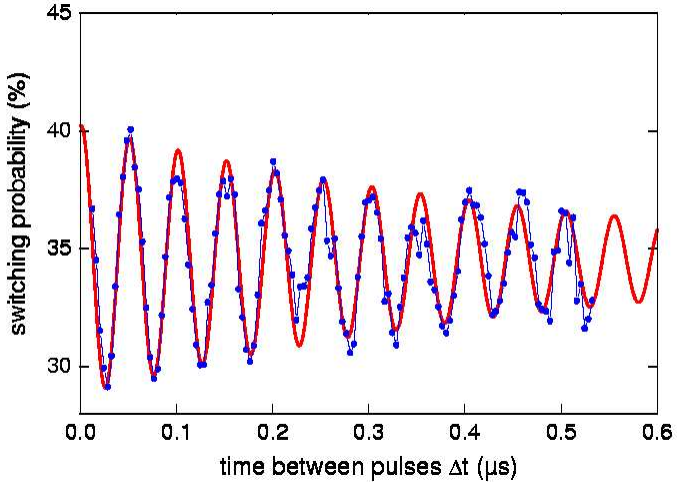


Figure 12: Ramsey fringe experiment on a quantronium sample at the optimal point. Two $\pi/2$ microwave pulses slightly out of resonance and separated by a time delay $t$ are applied to the gate. The oscillations of the switching probability (dots) at the detuning frequency probe decoherence. In this experiment, the cherence time was 500 $ns$, as estimated from an exponentially decaying cosine fit (full line). For the quantronium, Coherence times have been measured in the range $200-500$ $ns$ *(Quantronics group).*

more sophisticated pulse methods have been developed to probe coherence [41]. When the operating point is moved away from the optimal point at which decoherence is weak during a fraction of the delay between the two pulses of a Ramsey sequence, the signal gives access to decoherence at this new working point. The interest of this 'detuning' method is to perform qubit manipulations at the optimal working point without being hindered by decoherence. When the coherence time is too short for time domain experiments, the lineshape, which is the Fourier transform of the Ramsey signal, gives access to the coherence time. Coherence times obtained with all these methods on a single sample away from the optimal point in the charge and phase directions are indicated by full symbols in Fig. 14.

It is possible to shed further light on the decoherence processes and to fight them using the echo technique well known in NMR[35]. An echo sequence is a two $\pi/2$ pulse Ramsey sequence with a $\pi$ pulse in the middle, which causes the phase accumulated during the second half to be subtracted from the phase accumulated during the first half. When the noise-source producing the frequency fluctuation is static on the time scale of the pulse sequence, the echo does not decay. The observed echo decay times, indicated by open disks in Fig. 14, thus set constraints on the spectral density of the noise sources. In particular, these data indicate that the charge noise is significantly smaller than expected from the low frequency $1/f$ spectrum. Bang-bang suppression of dephasing, which generalizes the echo technique, could fight decoherence more efficiently[43].

### 7.3 Decoherence during driven evolution

During driven evolution, the density matrix is best defined using the eigenstate basis in the rotating frame. On resonance, these eigenstates are the states $|X\rangle$ and $|-X\rangle$ on the Bloch sphere. As in the laboratory frame, the decay of the density matrix involves relaxation and dephasing. The measurement of the relaxation time can be performed using the so-called spin locking technique in NMR[35], which allows one to measure the qubit polarisation after the preparation of the state $|X\rangle$. The coherence time during driven evolution is easily obtained from Rabi oscillations. Indeed, the initial state $|0\rangle$ is a coherent superposition of the eigenstates during driven evolution:

$|0\rangle = (|X\rangle + |-X\rangle)/\sqrt{2}$ .

The Rabi signal measured after a pulse of duration $t$ thus probes decoherence during driven evolution. The corresponding coherence time is longer than the coherence time during free evolu-

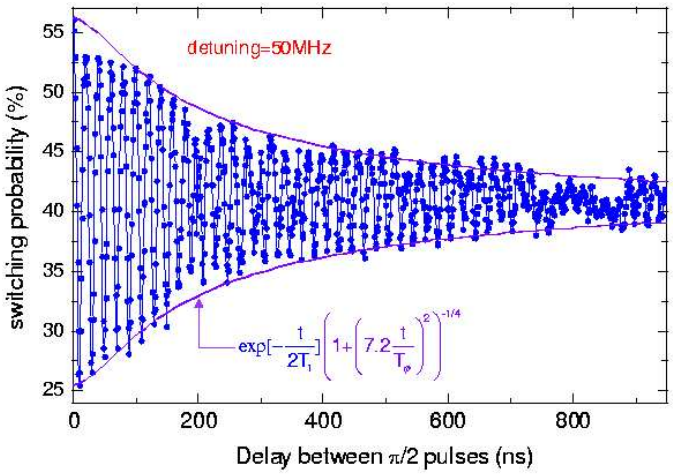


Figure 13: Symbols: Switching probability after a Ramsey two pulse sequence, as a function of the delay between pulses. The envelope is the best fit obtained with the static approximation.

tion because the driving field quenches the effect of the low frequency fluctuations that dominate dephasing during free evolution.

## 8 Qubit coupling schemes

### 8.1 First experimental results

Single qubit control and readout has been achieved for several Josephson qubits. Although the control accuracy and readout fidelity do not yet meet the requirements for quantum computing, the demonstration on such 'working' qubits of logic gates is now a main goal. Presently, only a few experiments have been performed on coupled qubits. A logic $C-NOT$ gate was operated in 2003 on charge qubits[44], but without single shot readout. The correlations between coupled phase qubits were measured recently using a single-shot readout[45]. In this experiment, a fixed coupling between two phase qubits with the same resonance frequency is implemented with a capacitor as shown in Fig. 15. Starting from state $|10\rangle$, the probabilities to obtain states $|10\rangle$ and $|01\rangle$ are then anticorrelated, as expected for a swapping interaction. The entanglement between two coupled qubits should however be investigated with better accuracy in order to probe the violation of Bell inequalities predicted by quantum mechanics. Only such an experiment could indeed test if collective degrees of freedom do obey quantum mechanics, and whether or not the entanglement decays as predicted from the known decoherence processes. We know discuss the different types of coupling schemes.

### 8.2 Tunable versus fixed couplings

In a processor, single qubit operations have to be supplemented with two qubit logic gate operations. During a logic gate operation, the coupling between the two qubits has to be controlled with great accuracy. For most solid state qubits, there is however no simple way to switch and to control the coupling. In the case of the superconducting qubits, controllable coupling circuits have been proposed [47], but fixed coupling Hamiltonians have been mostly considered and operated: capacitive coupling for phase, charge-phase and charge qubits, and inductive coupling for flux qubits. It is nevertheless possible to use a constant coupling Hamiltonian provided that the ef-

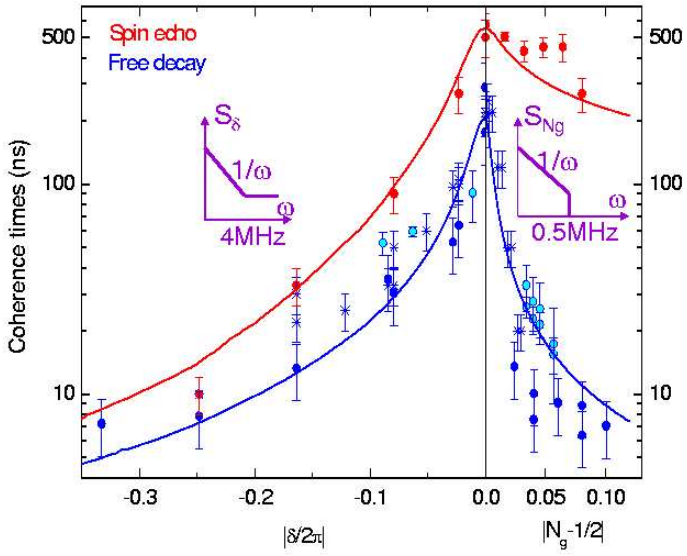


Figure 14: Coherence times $T_2$ and $T_{Echo}$ in a quantronium sample extracted from the decay of free evolution signals. The full and dashed lines are calculated using the the spectral densities depicted by the bottom graphs for the phase noise (left) and for the charge noise (right), respectively. *(Quantronics group).*

fective qubit-qubit interaction is controlled by other parameters. We now discuss all these coupling schemes.

The first demonstration of a logic gate was performed using a fixed Hamiltonian. The system used consisted of two Cooper pair boxes with their islands connected by a capacitance $C_C$. The coupling Hamiltonian is

$$H_{cc} = -E_{CC}(\widehat{N}_1 - N_{G1})(\widehat{N}_2 - N_{G2}) \tag{8}$$

where $E_{CC} = -E_{C1}E_{C2}C_C/(2e)^2$ is the coupling energy, smaller than the charging energy of the Cooper pair boxes. This Hamiltonian corresponds to changing the gate charges by $(E_{CC}/2E_{C1})\,/\,(\widehat{N}_2 - N_{G2})$ for qubit 1, and by $(E_{CC}/2E_{C2})\,/(\widehat{N}_1 - N_{G1})$ for qubit 2. The correlations between the two qubits predicted for this Hamiltonian have been probed, and a C-NOT logic gate was operated with this circuit[44].

In the uncoupled eigenstate basis, The Hamiltonian (8) contains both longitudinal terms of type $\widehat{\sigma}_{Z1}\widehat{\sigma}_{Z2}$ and transverse terms of type $\widehat{\sigma}_{X1}\widehat{\sigma}_{X2}$. At the double optimal point $N_{G1} = N_{G2} = 1/2$ , $\delta_1 = \delta_2 = 0$, the Hamiltonian (8) is however purely transverse $H_{CC} = \hbar\Omega_C\widehat{\sigma}_{X1}\widehat{\sigma}_{X2}$, with $\Omega_C = E_{CC}/\hbar \left|\left\langle 0_1 \left|\widehat{N}_1\right| 1_1\right\rangle\right| \left|\left\langle 0_2 \left|\widehat{N}_2\right| 1_2\right\rangle\right|$. When the two qubits have the same resonance frequency $\omega_{01}$, and when $\Omega_C \ll \omega_{01}$, the non-secular terms in $H_{CC}$ that do not commute with the single qubit Hamiltonian are ineffective, and the effective Hamiltonian reduces to:

$$H_{CC}^{\rm sec} = (\hbar\Omega_C)\ (\widehat{\sigma}_{+1}\widehat{\sigma}_{-2} + \widehat{\sigma}_{-1}\widehat{\sigma}_{+2})\ . \tag{9}$$

The evolution of the two qubits corresponds to swapping them periodically. More precisely, a swap operation is obtained at time $\pi/\Omega_C$. This gate is called *ISWAP* because of extra factors $i$:

$ISWAP\,|00\rangle = |00\rangle\,;\ ISWAP\,|10\rangle = -i\,|01\rangle\,;$

$ISWAP\,|01\rangle = -i\,|10\rangle\,;\ ISWAP\,|11\rangle = |11\rangle.$

At time $\pi/4\Omega_C$, the evolution operator corresponds to the gate $\sqrt{ISWAP}$, which is universal.

### 8.3 Control of the interaction mediated by a fixed Hamiltonian

The control of the qubit-qubit interaction mediated by a fixed Hamiltonian depends on the form of this Hamiltonian.

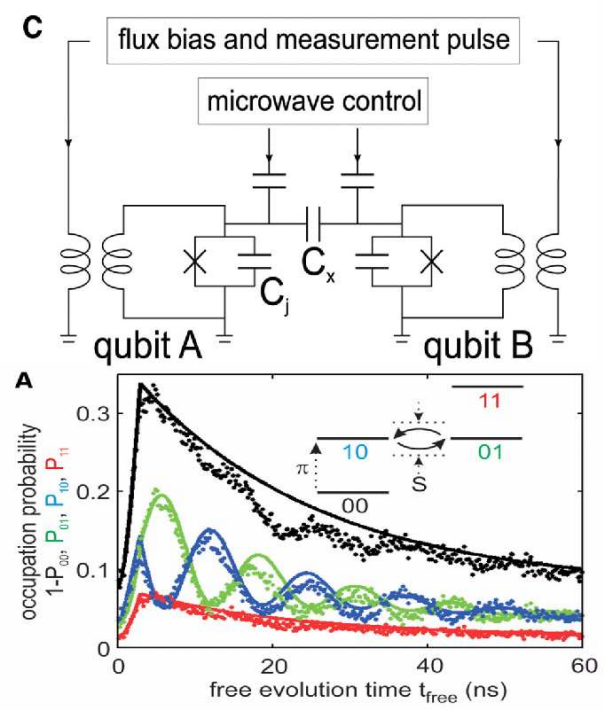


Figure 15: Two phase qubits are capacitively coupled and measured simultaneously after a free evolution time. The anticorrelation between the probabilities $P_{01}$ and $P_{10}$ demonstrate the swapping induced by the interaction (taken from [45] .

For a coupling of the form 9, the effective interaction can be controlled by varying the qubit frequencies since the qubits are affected only when their frequency difference is smaller than $\Omega_C$. This tuning strategy was recently applied to capacitively coupled phase qubits, in which the qubit frequency is directly controlled by the bias current of the junctions[7]. The correlations predicted by quantum mechanics between the readouts of the two qubits were observed[45]. The tuning strategy would be also well suited for coupling many qubits together through an oscillator[29]. The virtual exchange of photons between each qubit and the oscillator indeed yields a coupling of the form 9, which is efficient only when the two qubits are tuned. This coupling scheme yields truly scalable designs, whereas most of other schemes are limited to 1D qubit arrays, with nearest neighbor couplings. The coupling between a qubit and a resonator has already been demonstrated for the charge and flux qubits[46, 28].

Another method proposed recently consists in maintaining the qubits out of resonance, but in reaching an equivalent resonance condition in the presence of resonant microwave pulses applied to each one [48]. This method is based on a well known NMR protocol that aims at placing two different spin species 'on speaking terms'. In this scheme, the energy difference between the two qubits is exchanged with the microwave fields.

## 9 Conclusions and perspectives

Many solid state qubits have been proposed, and several of them have already demonstrated coherent evolution.

For semiconductor qubits, the coherent transfer of an electron between two dots has been demonstrated, and other promising designs are under investigation.

For superconducting qubits, single qubit control, single-shot readout, and a two-qubit logic gate have been achieved. Methods inspired from NMR have been applied to qubit manipulation

in order to improve manipulation robustness, and to probe decoherence processes. However, the lack of an efficient readout scheme and of robust two qubit gates still hinders the development of the field. New QND readout schemes are presently investigated in order to reach a higher readout fidelity. New qubit gates have been proposed, but none of them is as robust as classical gates used in ordinary classical processors. Currently, the coherence time, the readout fidelity, and the gate accuracy are insufficient to envision quantum computing. But how far from this goal are solid state qubits?

In order to use quantum error correcting codes, an error rate of the order of $10^{-4}$ for each logic gate operation is required. Presently, the gate error rates can be estimated at about a few % for single qubit gates, and at about 20% at best for two qubit gates. The present solid state qubits thus miss the goal by many orders of magnitude. When decoherence and readout errors are taken into account, quantum computing appears even more unrealistic. This is not, however, a reason to give up because conceptual and technical breakthroughs can be expected in this rather new field, and because no fundamental objection has been found. One should not forget that, in physics, everything which is possible is eventually done. Furthermore, quantum circuits provide new research directions in which fundamental questions on quantum mechanics can be addressed. The extension of quantum entanglement out of the microscopic world, and the location and nature of the frontier between quantum and classical worlds, are two of these essential issues. For instance, the accurate measurement of the correlations between two coupled qubits would indeed probe whether or not the collective variables of qubit circuits do follow quantum mechanics.

Our feeling is that, whatever the motivation, complex quantum systems and quantum machines are a fascinating field worth the effort.

## References

[1] M.A. Nielsen and I.L. Chuang, "*Quantum Computation and Quantum Information*" (Cambridge University Press, Cambridge, 2000.

[2] *Quantum Coherence and Information Processing* , edited by D. Esteve, J.M. Raimond, and J. Dalibard (Elsevier, 2004).

[3] S. Haroche, course 2 in ref. 2; M. Brune, course 3 in ref. 2.

[4] R. Blatt, H. Häffner, C.F. Ross, C. Becher, and F. Schmidt-Kaler, course 5 in ref. 2; D.J. Wineland, course 6 in ref. 2.

[5] C. Glattli, course 11 in ref. 2.

[6] M.H. Devoret and J. Martinis, course 12 in ref. 2.

[7] J. Martinis, course 13 in ref. 2.

[8] D. Vion, course 14 in ref. 2.

[9] B. E. Kane, *Nature* **393**, 133 (1998).

[10] T. Hayashi, T. Fujisawa, H. D. Cheong, Y. H. Jeong, and Y. Hirayama, *Phys. Rev. Lett.* **91**, 226804 (2003).

[11] J. Gorman, D.G. Hasko, and D.A. Williams, *Phys. Rev. Lett.* **95**, 090502 (2005).

[12] J. M. Elzerman, R. Hanson, L. H. Willems van Beveren, B. Witkamp, J. S. Greidanus, R. N. Schouten, S. De Franceschi, S. Tarucha, L. M. K. Vandersypen, and L.P. Kouwenhoven, *Quantum Dots: a Doorway to Nanoscale Physics*, in *Series: Lecture Notes in Physics,* **667**, Heiss, WD. (Ed.), (2005), and refs. therein.

[13] A. C. Johnson, J. R. Petta, J. M. Taylor, A. Yacoby, M. D. Lukin, C. M. Marcus, M. P. Hanson, A. C. Gossard, *Nature* **435**, 925 (2005).

[14] M.H. Devoret, in "*Quantum Fluctuations*", S. Reynaud, E. Giacobino, J. Zinn-Justin, eds. (Elsevier, Amsterdam, 1996), p.351.

[15] Guido Burkard, Roger H. Koch, and David P. DiVincenzo, *Phys. Rev. B* **69**, 064503 (2004).

[16] J. M. Martinis, S. Nam, J. Aumentado, and C. Urbina, *Phys. Rev. Lett.* **89**, 117901 (2002).

[17] J. E. Mooij, T. P. Orlando, L. Levitov, Lin Tian, Caspar H. van der Wal, and Seth Lloyd, *Science* **285**, 1036 (1999).

[18] I. Chiorescu, Y. Nakamura, C. J. P. M. Harmans, and J. E. Mooij, *Science* **299**, 1869 (2003).

[19] A. Cottet, D. Vion, P. Joyez, P. Aassime, D. Esteve, and M.H. Devoret, *Physica C* **367**, 197 (2002).

[20] D. Vion *et al.*, *Science* **296**, 886 (2002).

[21] A. Cottet, *Implementation of a quantum bit in a superconducting circuit*, PhD thesis, Université Paris VI, (2002); www-drecam.cea.fr/drecam/spec/Pres/Quantro/ .

[22] Y. Nakamura, Yu. A. Pashkin and J. S. Tsai, *Nature* **398**, 786 (1999).

[23] V. Bouchiat, D. Vion, P. Joyez, D. Esteve and M.H. Devoret, *Physica Scripta* **76**, 165 (1998); V. Bouchiat, PhD thesis, Université Paris VI, (1997), www-drecam.cea.fr/drecam/spec/Pres/Quantro/ .

[24] *Single Charge Tunneling*, edited by H. Grabert and M. H. Devoret (Plenum Press, New York, 1992).

[25] T. Duty, D. Gunnarsson, K. Bladh, and P. Delsing, *Phys. Rev.* **B 69**, 140503 (2004).

[26] R.J. Schoelkopf *et al.*, *Science* **280**, 1238 (1998).

[27] O. Astafiev, Yu. A. Pashkin, Y. Nakamura, T. Yamamoto, and J. S. Tsai, *Phys. Rev. Lett.* **93**, 267007 (2004).

[28] A. Wallraff, D. Schuster,.-I.; A. Blais; L. Frunzio; R.-S. Huang,- J. Majer, S. Kumar, S.M.Girvin, R.J. Schoelkopf, *Nature* **431**, 162 (2004); and p. 591 in ref. 2.

[29] Y. Makhlin, G. Schön and A. Shnirman, *Rev. Mod. Phy* **73**, 357 (2001).

[30] A. Lupascu, .J.M.Verwijs, R.N. Schouten, C.J.P.M. Harmans, and J.E. Mooij, *Phys. Rev. Lett.* **93**, 177006 (2004).

[31] I. Siddiqi, R. Vijay, F. Pierre, C. M. Wilson, M. Metcalfe, C. Rigetti, L. Frunzio,R.J. Schoelkopf, M. H. Devoret, D. Vion, and D. Esteve, *Phys. Rev. Lett.* **94**, 027005 (2005).

[32] I. Siddiqi, R. Vijay, F. Pierre, C. M. Wilson, M. Metcalfe, C. Rigetti, L. Frunzio, and M. H. Devoret, *Phys. Rev. Lett.* **93**, 207002 (2004).

[33] Mika A. Sillanpää, Leif Roschier, and Pertti J. Hakonen, *Phys. Rev. Lett.* **93**, 066805 (2004).

[34] I. Siddiqi etal., Cond-Mat 0507548. **93**, 207002 (2004).

[35] C.P. Slichter, *Principles of Magnetic Resonance*, Springer-Verlag (3rd ed: 1990).

[36] J. Jones, course 10 in ref. 2.

[37] L.M.K. Vandersypen and I.L. Chuang, quant-ph/0404064.

[38] D. Vion *et al.*, *Fortschritte der Physik* **51**, 462 (2003).

[39] E. Collin, G. Ithier, A. Aassime, P. Joyez, D. Vion, and D. Esteve, *Phys. Rev. Lett.* **93**, 157005 (2004).

[40] H.K. Cummins, G. Llewellyn, and J.A. Jones, *Phys. Rev. A* **67**, 042308 (2003).

[41] Ithier et al., *Phys. Rev. B.* **72**, 134519 (2005).

[42] K. B. Cooper, Matthias Steffen, R. McDermott, R. W. Simmonds, Seongshik Oh, D. A. Hite, D. P. Pappas, and John M. Martinis, *Phys. Rev. Lett.* **93**, 180401 (2004).

[43] G. Falci, A. D'Arrigo, A. Mastellone, and E. PaladinoPhys. Rev. A **70**, 040101 (2004); H. Gutmann, F.K. Wilhelm, W.M. Kaminsky, and S. Lloyd, *Quantum Information Processing* **3**, 247 (2004).

[44] T. Yamamoto et al., *Nature* **425**, 941 (2003), and Yu. Pashkin *et al.*, *Nature* **421**, 823 (2003).

[45] R. McDermott, R. W. Simmonds, Matthias Steffen, K. B. Cooper, K. Cicak, K. D. Osborn, Seongshik Oh, D. P. Pappas, and John M. Martinis, *Science* **307**, 1299 (2005).

[46] I. Chiorescu, P. Bertet, K. Semba, Y. Nakamura, C. J. P. M. Harmans, and J. E. Mooij, *Nature* **431**, 159 (2004).

[47] J. Q. You, Y. Nakamura, and F. Nori, *Phys. Rev. B* 71, 024532 (2005); J. Lantz, M. Wallquist, V. S. Shumeiko, and G. Wendin, *Phys. Rev. B* **70**, 140507 (2004).

[48] C. Rigetti, A. Blais, and M. H. Devoret *Phys. Rev. Lett.* 94, 240502 (2005).